Simultaneous Inhibition of LSD1 and TGF-β Enables Eradication of Poorly Immunogenic Tumors with anti-PD-1 Treatment

Wanqiang Sheng[1, 3, 4, *], Yi Liu[1, 3], Damayanti Chakraborty[1], Brian Debo[1], Yang Shi[1, 2, *]

[1]Division of Newborn Medicine and Epigenetics Program, Boston Children's Hospital, Harvard Medical School, Boston, MA 02115, USA

[2]Ludwig Institute for Cancer Research, University of Oxford, Oxford OX3 7DQ, UK

[3]These authors contributed equally

[4]Present address: Institute of Immunology, and Department of Respiratory Disease of The First Affiliated Hospital, Zhejiang University School of Medicine, Hangzhou, Zhejiang 310012, China

* Corresponding author

Corresponding authors:
Wanqiang Sheng
Address: Zhejiang University School of Medicine, 866 Yuhangtang Road, Hangzhou, Zhejiang 310012, China
Email: wanqiang_sheng@zju.edu.cn
Phone: (86)-571-8820-8275

Yang Shi
Address: Boston Children's Hospital, 300 Longwood Avenue, Boston, MA 02115, USA
Email: yang.shi@childrens.harvard.edu
Phone: (1)-617-919-3100

Running title: Combining LSD1 inhibition with dual PD-1/TGF-β blockade

Disclosure of Potential Conflicts of Interest
Y. Shi is a co-founder and equity holder of Constellation Pharmaceuticals, Inc., Athelas Therapeutics, Inc., and K36 Therapeutics, Inc., and holds equity of Imago Biosciences. Y. Shi is also a consultant for Active Motif, Inc. All other authors declare no competing financial interests.

ABSTRACT

Epigenetic regulators are a class of promising targets in the combination with immune checkpoint inhibitors for cancer treatment, but the impact of the broad effects of perturbing epigenetic regulators on tumor immunotherapy remains to be fully explored. Here we show that ablation of the histone demethylase LSD1 in multiple tumor cells induces TGF-β expression, which exerts an inhibitory effect on T cell immunity through suppressing the cytotoxicity of intratumoral $CD8^+$ T cells and consequently dampens the antitumor effect of LSD1 ablation-induced T cell infiltration. Importantly, concurrent depletion of LSD1 and TGF-β in combination with PD-1 blockade significantly increases both $CD8^+$ T cell infiltration and cytotoxicity, leading to eradication of poorly immunogenic tumors and a long-term protection from tumor re-challenge. Thus, combining LSD1 inhibition with blockade of TGF-β and PD-1 may represent a promising triple combination therapy for treating certain refractory tumors.

SIGNIFICANCE

Co-targeting LSD1 and TGF-β cooperatively elevates intratumoral $CD8^+$ T cell infiltration and unleashes their cytotoxicity, leading to tumor eradication upon anti-PD-1 treatment. Our findings illustrate a duality of epigenetic perturbations in immunotherapy and implicate the combination of LSD1 inhibition with dual PD-1/TGF-β blockade in treating certain poorly immunogenic tumors.

INTRODUCTION

The blockade of the immune inhibitory receptor PD-1 that mediates T cell dysfunction has led to unprecedented, long-lasting responses in a wide variety of cancers. However, outcomes of large clinical trials have clearly shown that anti-PD-1-directed immune checkpoint blockade (ICB) therapy has not been effective in a majority of cancer patients (1). Therefore, there are increasing interests and efforts in identifying potential targets for combination therapies to overcome tumor resistance to anti-PD-1 therapy. Genetic alterations frequently occur in cancer, some of which have been shown to suppress tumor immunogenicity and render unresponsiveness to PD-1 blockade (2). In addition to genetic alterations, epigenetic mis-regulation, another common feature of cancer, has emerged as a key regulator of tumor response to T cell immunity and anti-PD-1 therapy. For instance, the MHC-I can be functionally impaired by transcriptional silencing mediated by the Polycomb Repressive Complex 2 (PRC2) that catalyzes trimethylation of histone H3 lysine 27 (H3K27), which consequently attenuates tumor cell recognition by $CD8^+$ T cells. Thus, inhibition of PRC2 has been reported to restore anti-tumor immunity in MHC-I-low tumor models (3, 4). Recent studies have also identified DNMTs (DNA methyltransferases), LSD1 (H3K4me1/2 demethylase) and EZH2 (H3K27 methyltransferase) as suppressors of tumor responses to PD-1 blockade, and their individual inhibition can elicit tumor cell-intrinsic innate immune activation, thereby inflaming poorly immunogenic tumors with elevated T cell infiltration and sensitizing tumors to anti-PD-1 therapy (5-9). Together, these studies point to a promising therapeutic approach that uses epigenetic drugs to sensitize refractory tumors to anti-PD-1 treatment.

Given epigenetic regulators are broadly involved in controlling transcription programs, when they are targeted in tumor cells for the purpose of eliciting immune stimulatory effects in combination with anti-PD1, tumor cell-derived immunoregulatory cytokines, ligands or metabolites may also be altered in a way that exerts opposing effects and limits the combinatory effectiveness (10). For instance, TGF-β, which exerts potent suppression on immune surveillance, is secreted by tumor cells, in addition to multiple types of producers such as stromal cells, to enable immune evasion (11). Among a variety of immune suppressive mechanisms, TGF-β in the tumor microenvironment (TME) is known to inhibit the cytotoxicity of $CD8^+$ T cells (12), block T cell infiltration (13, 14) and promote Treg generation (15). In some cancers, the TGF-β pathway is epigenetically silenced (16, 17), therefore, when epigenetic regulators are targeted in combination with anti-PD-1 for treating such cancers, the TGF-β pathway might be re-activated and compromise the combinatory effect. Hence, a careful scrutinization of confounding effects of targeting epigenetic regulators may be warranted for developing effective combination therapies.

Our recent study has identified LSD1 as an inhibitor of tumor response to host immunity and PD-1 blockade, and its inhibition greatly sensitizes the refractory mouse B16/F10 melanoma to anti-PD-1 therapy (8). However, this combination did not result in a complete eradication of established tumors, similar to other combinations targeting epigenetic regulators together with ICB (6, 18, 19). In this study, we investigated the underlying mechanisms and identified TGF-β induction as a side-effect of LSD1 ablation in tumor cells, which suppresses $CD8^+$ T cell cytotoxicity and blocks T cell infiltration in response to PD-1 blockade. Accordingly, concurrent depletion of LSD1 and TGF-β renders these refractory tumors superiorly responsive to anti-

PD-1 treatment, accompanied by tumor rejection. Importantly, this study also suggests that targeting LSD1 may sensitize certain otherwise refractory tumors to the emerging dual PD-1/TGF-β blockade therapy, which potentially extends the utility of this triple combination to the treatment of poorly immunogenic tumors.

RESULTS

LSD1 Ablation in Tumor Cells Induces TGF-β Expression That Does Not Interfere with the Simultaneous IFN Activation

We recently reported that LSD1 inhibition enhances tumor immunogenicity through activating the dsRNA-IFN pathway, resulting in an elevated T cell infiltration in poorly immunogenic tumors, which sensitizes tumors to PD-1 blockade therapy (8). Although LSD1 null melanoma growth was greatly inhibited in response to anti-PD-1 treatment, tumors were not eradicated (8). Unexpectedly, further analyses showed that the mean fluorescence intensity (MFI) of the cytotoxic molecule Granzyme B (GzmB) in individual $CD8^+GzmB^+$ tumor-infiltrating lymphocytes (TILs) was moderately decreased in LSD1 null tumors (**Supplementary Fig. S1A**), although the percentages of $GzmB^+$ cells remained unchanged (8). We therefore hypothesized that certain immune suppressive molecules originated from tumor cells might be concurrently induced when LSD1 was inhibited, and such molecules could suppress the cytotoxicity of $CD8^+$ TILs and compromise the immune stimulatory effect of targeting LSD1. To search and identify such immune suppressive molecules, we re-examined the transcriptomic data obtained from *ex vivo* tumors (8). The Gene Ontology (GO) analysis of the upregulated genes caused by LSD1 loss, however, did not successfully identify any candidate pathways of interest as significant hits (**Supplementary Fig. S1B; Supplementary Table S1**). We then interrogated a list of individual genes with well-documented roles in suppressing T cell immunity directly or indirectly through dendritic cells (DCs) (10, 20, 21), with two filtering criteria: 1) gene transcripts were reliably detected in LSD1-deficient B16 tumor cells (logCPM > 1) and 2) gene expression was significantly induced by LSD1 ablation compared with control

(FC > 1.5 and FDR < 0.05). This analysis uncovered two hits, the *Tgfb* subfamily and *Csf1* (encoding M-CSF) (**Supplementary Fig. S1C-S1E; Supplementary Table S2**).

We next investigated whether and how TGF-β subfamily members (TGF-βs) were regulated by LSD1 in tumor cells. As expected, LSD1 ablation in *in vitro* cultured B16/F10 (B16 in short) cells strongly induced the Tgfb1 transcript level, and also moderately increased Tgfb2 and Tgfb3 (**Fig. 1A**). This upregulation was largely suppressed when LSD1 was re-introduced into the cells (**Fig. 1A**). We further quantified the secreted TGF-β1 by ELISA and showed that B16 cells, though normally secreting a low amount of TGF-β1 (22), became potent TGF-β1 producers upon LSD1 ablation (**Fig. 1B**). The ablation of CoREST (encoded by *Rcor1*), a key component of the LSD1/CoREST complex, also led to the upregulation of Tgfb1 as well as Serpine1, a well-characterized TGF-β downstream gene (**Fig. 1C**). Given LSD1 ablation strongly activated type 1 IFN pathway (8), we also tested the effect of autocrine IFNs on TGF-β expression and found that IFN-β depletion did not attenuate TGF-β induction (**Supplementary Fig. S2A** and **S2B**). Instead, it is likely that LSD1 directly regulates TGF-β upregulation as we found it bound to the promoter region of *Tgfb1* gene and its ablation increased active histone marks (**Supplementary Fig. S2C**). The induction of Tgfb subfamily members in response to LSD1 ablation occurred in multiple types of cancer cells of both mouse and human origins, including melanoma, lung carcinoma and breast cancer (**Supplementary Fig. S2D-S2L**), suggesting that Tgfb expression is generally repressed by LSD1 across different tumor types.

We next asked if TGF-β upregulation affected IFN activation in LSD1 null tumor cells. We deleted all three *Tgfb* genes in LSD1 null B16 cells by CRISPR/Cas9 and confirmed the

removal of functional alleles of *Tgfb* genes by sequencing, transcript detection and protein quantification (**Supplementary Fig. S3A-S3C**). *Serpine1*, a reporter gene for TGF-β pathway activation, was significantly induced in LSD1-deficient B16 cells, but this induction was by and large abolished in Lsd1/Tgfb quadruple knockout (QKO) cells (**Supplementary Fig. S3D**), providing an additional line of evidence for the loss of TGF-β pathway activity in these cells. We found that LSD1 ablation-stimulated IFN activation was largely unaffected by the elevated TGF-β expression, as IFNs and Interferon Stimulated Genes (ISGs) showed comparable expression between Lsd1 KO and Lsd1/Tgfb QKO B16 cells (**Fig. 1D** and **E**). Taken together, these results demonstrate that LSD1 ablation in tumor cells induces TGF-β expression, which does not interfere with the simultaneous IFN activation.

Abrogation of TGF-β Induction Potentiates the anti-Tumor T cell Immunity Stimulated by LSD1 Ablation

We next investigated the *in vivo* biological significance of the induced TGF-β expression in LSD1-depleted tumors. To this end, we transplanted four groups of B16 tumors (Scramble, Lsd1 KO, Tgfb TKO and Lsd1/Tgfb QKO) into syngeneic, immunocompetent mice for tumor growth. While abrogation of all three TGF-βs alone had no observable effect on tumor growth, abrogation of TGF-βs in LSD1 null tumors showed a moderate but statistically significant effect on restraining tumor growth, evidenced by the further delayed growth of Lsd1/Tgfb QKO tumors compared with Lsd1 KO tumors and further extended survival **(Fig. 1F** and **G**). Thus, in wildtype B16 tumors with a low basal level of TGF-β expression ((22); **Fig. 1H**), tumor cell-derived TGF-βs seemed to have neglectable effects on overall tumor growth. However, when LSD1 was ablated in tumor cells, TGF-β1 secretion was induced to a significant level (**Fig.**

1H), which exerted an immune suppressive effect and counteracted the antitumor effect of LSD1 inhibition. Importantly, there were no discernable growth difference between Lsd1/Tgfb QKO and scramble tumors in the immunodeficient T cell receptor α (TCRα) KO mice (**Fig. 1I**), suggesting that the antitumor effect resulting from the abrogation of TGF-β induction in LSD1 null tumors relies on T cell immunity. To further determine the roles of $CD8^+$ versus $CD4^+$ T cells in mediating the antitumor effect of Lsd1/Tgfb ablation, we performed antibody-mediated depletion of either $CD8^+$ or $CD4^+$ T cells. We found that the growth difference between Lsd1/Tgfb QKO and scramble tumors was largely diminished by the depletion of $CD8^+$ but not $CD4^+$ T cells (**Fig. 1J**), suggesting that it is mainly $CD8^+$ T cells that mediate the anti-tumor effect of TGF-β removal in LSD1 null tumors.

In addition to the subcutaneous tumor growth model, we also evaluated the role of TGF-β induction in a lung metastasis model, since TGF-βs are well documented to promote tumor cell epithelial–mesenchymal transition (EMT), invasion and metastasis (11). B16 cells were intravenously injected into mice to allow the circulation of tumor cells into lungs. The analysis of lung colonization by tumors showed that LSD1 loss inhibited B16 tumor metastasis only in wildtype (WT) but not TCRα KO mice (**Supplementary Fig. S4A** and **S4B**), suggesting that LSD1 ablation-elicited T cell immunity is critical in controlling tumor metastasis. This observation is opposite to a previous report where LSD1 inhibition has been shown to increase breast cancer metastasis (23). The difference could be due to the use of xenograft (23) versus immunocompetent syngeneic models (this study), or due to different tumor types. The concurrent abrogation of TGF-βs in LSD1 null tumors imparted further inhibitory effect on lung metastasis, evidenced by the observation that Lsd1/Tgfb QKO tumors showed the least lung

metastasis compared with either Lsd1 KO or Tgfb TKO tumors (**Supplementary Fig. S4A**). Importantly, the cooperative effect between concurrent LSD1 and TGF-β ablation on controlling tumor lung metastasis also depended on T cell immunity, because the absence of T cells completely abrogated this effect (**Supplementary Fig. S4B**). Of note, TGF-β ablation alone modestly suppressed tumor lung metastasis and this inhibitory effect was only observed when T cells were present (**Supplementary Fig. S4A** and **S4B**). In summary, these findings suggest that tumor cell-derived TGF-βs, unintentionally induced when LSD1 is removed in tumor cells, may compromise the immune stimulatory effect of LSD1 inhibition. Thus, blockade of TGF-βs could potentiate the antitumor effect of LSD1 inhibition in certain tumors.

Abrogation of TGF-β Induction Unleashes CD8$^+$ T Cell Cytotoxicity in LSD1 Null Tumors

To understand how the TGF-β induction compromised the antitumor CD8$^+$ T cell immunity elicited by LSD1 ablation, we analyzed lymphocyte infiltration in the TME. As previously reported (8), LSD1 ablation strongly increased CD8$^+$ T cell infiltration, whereas the concurrent ablation of TGF-βs in LSD1 null tumors resulted in no further increase (**Fig. 2A**). This was expected in some way, because IFN pathway activation, which is essential for LSD1 ablation-stimulated CD8$^+$ T cell infiltration (8), was comparable between Lsd1 KO and Lsd1/Tgfb QKO tumor cells (**Fig. 1D**). Other lymphocytes were also by and large numerically comparable between Lsd1 KO and Lsd1/Tgfb QKO tumors (**Supplementary Fig. S5A-S5E**), as well as in tumor draining lymph nodes (TdLNs) of tumor-bearing mice **(Supplementary Fig. S6A-S6H**). Of note, although TGF-β plays a well-documented role in promoting Treg cells (24), we did not detect an obvious alteration in Treg cell frequency when TGF-β levels were fluctuating in the TME (**Supplementary Fig. S5D; Fig. 1H**). This phenomenon is not unique to our tumor model,

as previous studies also reported that TGF-β blockade by neutralizing antibodies did not change Treg cells in the TME (14). Thus, the secreted TGF-βs by LSD1 null B16 tumors counteract the antitumor immunity in a way other than altering T cell infiltration.

We next assessed the functional profile of $CD8^+$ TILs, on which the induced TGF-βs might impact. The proliferation of $CD8^+$ TILs was analyzed by measuring the expression of Ki-67, a cell proliferation marker, which appeared to be unaltered by either LSD1 ablation or concurrent TGF-β ablation (**Fig. 2B**). In addition, $CD8^+$ TILs isolated from scramble, Lsd1 KO and Lsd1/Tgfb QKO B16 tumors had comparable PD-1 expression (**Fig. 2C**), indicating similar levels of T cell activation. In contrast, we found that the percentage of GzmB-expressing cells among $CD8^+$ TILs was significantly increased in Lsd1/Tgfb QKO tumors compared with those in scramble or Lsd1 KO tumors (**Fig. 2D**). Importantly, the GzmB protein level (measured by MFI) in individual $CD8^+GzmB^+$ TILs, which was suppressed in Lsd1 KO tumors, was restored when tumor cell-derived TGF-βs were concurrently abrogated (**Fig. 2E**). As a control, TGF-β ablation alone in B16 tumor cells had no overt effect on $CD8^+$ T cell infiltration, proliferation or GzmB expression (**Supplementary Fig. S7A-S7D**), in line with the unaltered tumor growth of Tgfb TKO tumors (**Fig. 1F**).

To further characterize $CD8^+$ TILs in the TME of genetically modified B16 tumors, we used RNA-seq to interrogate their transcriptional phenotype. LSD1 ablation in B16 tumor cells appeared to have a minor impact on the gene expression profile of $CD8^+$ TILs and we only found 25 and 10 genes down- and up-regulated, respectively, in $CD8^+$ TILs from Lsd1 KO tumors compared with those from scramble tumors (**Supplementary Fig. S8A; Fig. 2F**). When

Tgfb genes were deleted on top of Lsd1 KO in B16 tumors, more genes were significantly upregulated in $CD8^+$ TILs (119 genes for QKO versus scramble or 99 genes for QKO versus Lsd1 KO alone) (**Fig. 2F**). As a control, Tgfb ablation alone only elevated the expression of 20 genes (**Fig. 2F**). These data suggest that ablation of Lsd1 and Tgfb in B16 tumors cooperatively induce gene expression in $CD8^+$ TILs, which was supported by the result obtained from comparing the expression of a list of genes among all samples (**Fig. 2G**). The GO enrichment analysis revealed that the upregulated genes (QKO versus KO) were significantly enriched in GO terms related to innate immune response and granzyme activity (**Fig. 2H**), and a list of representative genes are shown in **Supplementary Fig. S8B**. Consistently, the analysis of a panel of T cell cytotoxicity-related molecules showed that the transcripts of several granzyme genes, whose expression appeared to be suppressed in Lsd1 KO tumors, were elevated by the concurrent ablation of Lsd1 and Tgfb (**Fig. 2I**). The expression of Fasl, Ifng and Tnf by $CD8^+$ TILs, however, did not appear to be much affected by Lsd1 or/and Tgfb depletion in tumors (**Fig. 2I-K**). These data thus demonstrate that granzyme expression by $CD8^+$ TILs is selectively and transcriptionally suppressed in Lsd1 KO tumors as a result of TGF-β induction.

Additionally, we analyzed the abundance and phenotype of myeloid cells in the TME, which could also be affected by TGF-β induction. We found that the abundances of DCs and macrophages were comparable between Lsd1 KO and Lsd1/Tgfb QKO tumors, while the $Gr1^{hi}$ myeloid-derived suppressor cells (MDSCs) showed a moderately higher abundance in Lsd1/Tgfb QKO than Lsd1 KO tumors (**Supplementary Fig. S9A-S9E**). Notably, the modest suppression of CD86 expression in two subsets of DCs and the upregulation of arginase

expression in MDSCs detected in LSD1 null tumors can be restored by simultaneous TGF-β ablation (**Supplementary Fig. S9F-S9I**), implicating an immune suppressive effect of TGF-β induction through targeting innate immune cells. Collectively, these results suggest that TGF-β induction in LSD1 null tumors compromises the antitumor effect of $CD8^+$ TILs through suppressing their cytotoxicity, which might involve a direct effect of TGF-β on T cells and/or an indirect effect mediated by innate immune cells.

TGF-β Receptor Signaling in αβ T cells is Necessary for Suppressing $CD8^+$ T Cell Cytotoxicity in Response to LSD1 Ablation-Induced TGF-βs

To determine if T cells were the primary targets of tumor cell-derived TGF-βs in LSD1 null tumors, we specifically blocked the TGF-β pathway in T cells using CD4-dnTGFBRII transgenic mice, which express a dominant negative TGF-β receptor (dnTβRII) on αβ T cells that attenuates T cell response to TGF-β signals (25). We speculated that if LSD1 ablation-induced TGF-βs act on T cells, the growth difference between Lsd1 KO and Lsd1/Tgfb QKO tumors observed in WT mice should be diminished when they were implanted in the dnTβRII transgenic mice. We found when Lsd1 KO tumors were implanted in dnTβRII transgenic mice, their growth was significantly suppressed to a level even slower than of Lsd1/Tgfb QKO tumors (**Fig. 3A**). Importantly, the expression of GzmB by $CD8^+$ TILs in Lsd1 KO tumors was increased by the presence of dnTβRII to a similar level as those in Lsd1/Tgfb QKO tumors, whereas GzmB expression by $CD8^+$ TILs in scramble and Lsd1/Tgfb QKO tumors remained largely unchanged (**Fig. 3B** and **C**). Of note, scramble and Lsd1/Tgfb QKO tumors with low levels of TGF-β expression also responded to the blockade of TGF-β receptor signaling in T cells by exhibiting a reduced tumor growth (**Fig. 3A**), which was possibly due to the significant

reduction of Treg cells (**Fig. 3D** and **E**), considering the critical role of TGF-β pathway in Treg induction and maintenance (24). Thus, these results suggest that TGF-β induction in response to LSD1 loss in tumor cells acts on αβ T cells and ultimately suppresses the cytotoxicity of $CD8^+$ TILs, although the detailed underlying mechanism remains to be further explored.

TGF-β family proteins are known to play a tumor cell growth inhibitory role by suppressing cell cycle progression, promoting differentiation and inducing apoptosis (11). Therefore, the slower growth of Lsd1 KO tumors compared with Lsd1/Tgfb QKO tumors in dnTβRII transgenic mice, where TGF-βs' effect on T cells are blocked, could be due to a growth inhibitory effect of TGF-βs on B16 tumor cells. Indeed, we found that the B16 cell growth inhibition as a result of Lsd1 KO was partially rescued by the concurrent ablation of *Tgfb* genes (**Supplementary Fig. S10A**), and the addition of exogenous TGF-β1 to the cultured Lsd1/Tgfb QKO cells re-installed the growth inhibition (**Supplementary Fig. S10B**). To identify the mechanism by which TGF-β upregulation inhibited Lsd1 KO B16 cell growth, we analyzed cell cycle progression and apoptosis. We detected a modest but statistically significant G1 arrest in Lsd1 KO cells, which was rescued by the concurrent Tgfb deletion (**Supplementary Fig. S10C** and **S10D**). In addition, Annexin V staining was elevated in Lsd1 KO but not Lsd1/Tgfb QKO cells (**Supplementary Fig. S10E** and **S10F**). These results demonstrate that TGF-β upregulation caused by LSD1 ablation inhibits *in vitro* B16 cell growth at least in part through suppressing cell cycle progression and promoting apoptosis.

To further confirm the growth inhibitory effect of TGF-βs on Lsd1 KO B16 tumor cells *in vivo*, we ectopically expressed a TGF-β dominant negative receptor (TGFβRII-DN) on the surface of

Lsd1 KO B16 cells (**Fig. 3F**), which did not interfere with TGF-β expression but rendered B16 cells unresponsive to TGF-β signals (**Fig. 3G**). When implanted in WT mice, Lsd1 KO tumors expressing TGFβRII-DN grew significantly faster than those responsive to TGF-β signals (**Fig. 3H**). Thus, TGF-βs induced by LSD1 ablation in B16 tumors play at least two opposing roles: primarily, paracrine TGF-βs play a pro-tumor role by acting on T cells and suppressing $CD8^+$ T cell cytotoxicity, which compromises the antitumor effect of LSD1 loss; secondarily, autocrine TGF-βs play an antitumor role by acting on tumor cells and inhibiting cell survival/proliferation.

Anti-PD-1 Treatment Eradicates LSD1 Null Tumors When TGF-β is Concurrently Blocked, Resulting in Immunity Against Tumor Re-challenge

Recent studies have identified TGF-β as a critical inhibitor of tumor response to anti-PD-1 therapy mainly through expelling T cell infiltration (13, 14). In the poorly immunogenic B16 tumor model, neither Tgfb deletion alone nor their deletion on top of Lsd1 loss altered T cell infiltration in the TME (**Fig. 2A; Supplementary Fig. S7A**); instead, a critical role of TGF-β lies in suppressing $CD8^+$ T cell cytotoxicity, which might be responsible for the incomplete response of LSD1 null tumors to PD-1 blockade. To test this possibility, we examined the response of Lsd1/Tgfb QKO tumors to anti-PD-1 treatment and found that those tumors showed profound growth control in response to PD-1 blockade and, excitingly, ~44% of QKO tumors were rejected by PD-1 blockade without recurrence up to 60 days (**Fig. 4A** and **B**). This is in stark contrast to our previous report that LSD1 null B16 tumors, though reduced, could not be completely rejected by anti-PD-1 treatment (8).

To determine whether mice, which rejected Lsd1/Tgfb QKO tumors upon anti-PD-1 treatment, had developed immunity, surviving mice were re-challenged with WT B16 tumors on the left hind flank 60 days after clearance of the primary tumors. While naïve, age-matched control mice all grew tumors and reached the end-point within 30 days, 5 out of 6 mice cured by Lsd1/Tgfb ablation plus anti-PD-1 treatment rejected secondary B16 tumors (**Supplementary Fig. S11A** and **S11B**). Mice that survived from B16 re-challenge were subsequently challenged with the irrelevant MC38 colorectal adenocarcinoma on the right front flank 60 days after secondary tumor clearance. In contrast to the re-challenge of B16 tumors, MC38 tumors grew similarly in those mice compared with their counterparts in the naïve age-matched mice (**Supplementary Fig. S11C**). These results suggest that tumor bearing-mice cured by Lsd1/Tgfb ablation plus anti-PD-1 treatment may have developed immunological memory.

Next, we sought to substitute genetic perturbation of Tgfb with systemic delivery of TGF-β blocking antibodies. While anti-PD-1 already suppressed LSD1 null tumor growth, the inclusion of anti-TGF-β in the combination exerted additional inhibitory effect on tumor growth, leading to the rejection of 2 out of 9 tumors (**Fig. 4C**). Notably, although single treatment with anti-PD-1 or anti-TGF-β had no overt effect on scramble B16 tumors, their combination gave rise to a synergistic effect on restraining tumor growth (**Fig. 4C**). To explore the generalizability of our study, we performed a similar tumor growth experiment in D4m.3A melanoma model, and found that, most impressively, the combination of anti-TGF-β and anti-PD-1 drastically increased the rejection rate of LSD1 null tumors compared with anti-PD1 alone (80% versus 20%), whereas this combination had no obvious effect on scramble tumor growth (**Fig. 4D** and **E**). These results demonstrate an inhibitory role of TGF-βs that compromises a full response of

LSD1 null tumors to anti-PD-1 treatment, highlighting the importance of blocking TGF-β pathway when LSD1 is targeted in this combination immunotherapy.

To further clarify the mechanistic roles of LSD1 ablation, TGF-β blockade and PD-1 blockade in their cooperative effect on tumor growth control, we analyzed the immune phenotype of B16 tumors in response to single or different combinatory treatments. We found that LSD1 loss played a major part in elevating $CD8^+$ T cell infiltration as did the combination of PD-1 and TGF-β blockade, but undesirably compromised the cytotoxicity (GzmB MFI) of $CD8^+$ TILs, even when PD-1 blocking antibodies were applied (**Fig. 4F-H**). In line with the genetic data (**Supplementary Fig. S7A**, **S7C** and **S7D; Fig. 2E**), TGF-β blockade alone had no overt effect on either T cell infiltration or $CD8^+$ T cell cytotoxicity in scramble B16 tumors, but helped restore the cytotoxicity (GzmB MFI) of $CD8^+$ TILs in LSD1 null tumors (**Fig. 4F** and **H**). PD-1 blockade alone significantly increased the cytotoxicity ($GzmB^+$ percentage) of $CD8^+$ TILs, but had limited impact on T cell infiltration in our experimental settings (**Fig. 4F** and **G**). Importantly, the triple combination of LSD1 ablation, PD-1 blockade and TGF-β blockade cooperatively elevated T cell infiltration while unleashing $CD8^+$ T cell cytotoxicity (**Fig. 4F**-**H**), leading to the improvement of tumor rejection. With respect to T cell infiltration, Lsd1 ablation likely worked through inflaming poorly immunogenic tumors for better T cell recruitment, since it did not affect the proliferative response of $CD8^+$ TILs to dual PD-1/TGF-β blockade (**Fig. 4I**). As a control, the frequencies of Treg cells were found to be mostly comparable between different groups of treatment (**Fig. 4J**). TGF-β inhibition by genetic depletion seemed to be more effective than blocking antibodies on unleashing T cell cytotoxicity when applied together with the PD-1 blocking antibodies (**Fig. 4K** and **L**). In summary, LSD1 ablation, TGF-β

blockade and PD-1 blockade cooperatively potentiate both T cell infiltration and cytotoxicity that enables the eradication of certain poorly immunogenic tumors.

DISCUSSION

The combination of epigenetic therapy and immunotherapy represents an emerging approach for cancer treatment (26). Our present study shows that, when the histone demethylase LSD1 is targeted for promoting T cell infiltration in the poorly immunogenic B16 and D4m.3A tumors, the immune suppressive TGF-βs are concurrently induced to a significant level that suppresses $CD8^+$ T cell cytotoxicity and also impedes the combinatory effect of LSD1 ablation and PD-1 blockade through restraining both $CD8^+$ T cell cytotoxicity and infiltration. Importantly, LSD1 depletion appears to enable and significantly improve the response of certain poorly immunogenic tumors to dual PD-1/TGF-β blockade, which is currently being explored as a new combination treatment strategy (27). Our findings thus raise a promising strategy that combines LSD1 inhibition with the blockade of TGF-β and PD-1 for treating certain poorly immunogenic or “cold” tumors.

The regulatory role of LSD1 in TGF-β expression was first uncovered a decade ago where LSD1 downregulation, which was reported in breast carcinomas, led to the upregulation of TGF-β and promoted breast cancer metastasis in xenograft tumor models (23). However, the biological significance of this initial report was not fully investigated. In fact, LSD1 is commonly upregulated in various cancer types and considered to mostly play a tumor-promoting role through multiple mechanisms including maintaining cancer stem cell renewal, sustaining tumor cell proliferation and suppressing antitumor immunity (28), which makes LSD1 a promising target for cancer treatment. Our study identifying a suppressive effect of LSD1 on TGF-β expression is consistent with this previous report, and we have further extended this regulation to multiple types of tumor cells. More importantly, our study using syngeneic tumor models has

investigated an unexplored role of this regulation, in which LSD1 inhibition-induced TGF-βs suppress $CD8^+$ T cell cytotoxicity in the TME and consequently counteract the antitumor effect of LSD1 inhibition-stimulated $CD8^+$ T cell infiltration. The TGF-β signaling pathway in αβ T cells was involved in mediating the immune suppressive effect of tumor cell-derived TGF-βs. Although a direct inhibitory effect of TGF-βs on $CD8^+$ T cells has been previously reported (12), we could not rule out the possibility that $CD4^+$ T cells might also be involved in mediating the suppression of $CD8^+$ T cell cytotoxicity in response to the elevated TGF-βs. Meanwhile, we also observed an antitumor effect of LSD1 inhibition-induced TGF-βs accomplished through inhibiting tumor cell survival/proliferation (**Supplementary Fig. S10**). This is not surprising, since TGF-β is a pleiotropic cytokine known to play both antitumor and pro-tumor roles depending on tumor types, tumor stages, genetic and epigenetic properties, as well as the TME (11, 29). Under the circumstance of targeting LSD1 for controlling B16 tumor growth, the pro-tumor effect of the induced TGF-βs outweighed its antitumor effect (**Fig. 1F**), highlighting the importance of blocking TGF-β in conjunction with LSD1 inhibition.

The development of cancer therapies by targeting the TGF-β pathway has faced drawbacks, partly because of the antitumor role of the TGF-β pathway in certain tumor contexts, which is supported by longstanding evidence (11), as well as safety issues observed in previous clinical trials (30). The fact that the TGF-β pathway plays a significant part in suppressing antitumor immunity points to a therapeutic approach combining TGF-β pathway inhibition and immunotherapy, which has gained renewed attention since ICB was demonstrated to be successful. The combinatorial effect of TGF-β pathway inhibition and PD-(L)1 blockade varies across a range of reported syngeneic tumor models. In immunogenic but “immune-excluded”

tumor models including EMT6 and MC38, where TGF-β signaling in fibroblasts is thought to be a key barrier for T cell penetration into tumor parenchyma, co-targeting PD-L1 and TGF-β has shown superior tumor eradication (14, 31). However, in poorly immunogenic tumor models such as KPC1, TC1 and 4T1, there is a lack of persuasive combinatorial effect of anti-PD-L1 and LY364947 (a TGFBR-I inhibitor) (22), as well as between anti-PD-1 and anti-TGF-β in the absence of vaccination (32) or radiation therapy (33), presumably due to low mutational burdens or the absence of T cell recognition. Indeed, in our study, the poorly immunogenic B16/F10 melanoma showed a moderate response and D4m.3A melanoma showed no response to anti-TGF-β/anti-PD-1 treatment (**Fig. 4C** and **D**). The lack of a robust response could be overcome by including LSD1 inhibition in the combination (**Fig. 4C** and **D**), as this triple combination can potentiate both T cell infiltration and cytotoxicity.

Our study centers on identifying immune suppressive mediators that are unintentionally induced by LSD1 inhibition, which then counteract the immune stimulatory effect of LSD1 inhibition and impede the synergistic effect of combining LSD1 inhibition and PD-1 blockade in tumor control. The findings from this study illustrate a duality of epigenetic perturbations in the combination with ICB therapy, highlighting the importance of thorough examinations of transcriptional programs and biological processes regulated by epigenetic regulators under investigation for the purpose of provoking immune responses in combination immunotherapy. Therefore, our findings may be relevant when small molecules targeting other epigenetic regulators are used in immunotherapy. In summary, our findings suggest a triple combination strategy that combines LSD1 inhibition, TGF-β blockade and PD-1 blockade for treating certain ICB-refractory tumors. Extensive future studies are warranted to discover biomarkers for

tumors that respond to this combination therapy in order to further develop this new cancer treatment strategy.

Authors' Contributions

W. Sheng and Y. Shi conceived the project; W. Sheng and Y. Liu designed and performed all experiments with help from D. Chakraborty and B. Debo under the supervision of Y. Shi; W. Sheng analyzed the RNA-seq data; W. Sheng, Y. Liu and Y. Shi wrote the manuscript; all authors read the manuscript.

Acknowledgments

We thank all the Shi lab members for discussion and suggestions. We thank Arlene Sharpe, David Fisher and Glenn Dranoff for sharing cell lines. We thank the Department of Immunology's Flow Cytometry Facility (HMS) for assistance on flow cytometric analysis. This work was supported by funds from the NIH (R35 CA210104), Boston Children's Hospital and Ludwig Institute for Cancer Research. Y. Shi is an American Cancer Society Research Professor.

METHODS

Cell Culture

All cancer cell lines were cultured in DMEM growth medium (Gibco, cat#1195) supplemented with 10% heat-inactivated FBS (Gemini Bio, cat#900-108) and 1% penicillin/streptomycin (Gibco, cat#15140122) in a 5% CO_2 incubator at 37 °C. B16/F10, D4m.3A and MC38 cell lines were from Drs. Glenn Dranoff (Novartis), David Fisher (MGH) and Arlene Sharpe (HMS), respectively. These cell lines were confirmed to be mycoplasma-free by the Universal Mycoplasma Detection Kit (ATCC® 30-1012K™) according to the manufacturer's instructions. T cell stimulation were performed in R10 medium (RPMI-1640 supplemented with 10% FBS, 1% penicillin/streptomycin, 12 mM HEPES and 50 μM β-mercaptoethanol).

Gene Deletion by CRISPR/Cas9

The guide RNA (gRNA) oligos targeting mouse *Tgfb1*, *Tgfb2*, *Tgfb3* and *Rcor1* (encoding CoREST) (sequences listed in **Supplementary Table S3**) were annealed and cloned into a lenti-CRISPR-v2-Puromycin$^+$ vector (Addgene, cat# #52961), respectively. Lentivirus carrying lenti-CRISPR plasmid was prepared by co-transfecting HEK293T cells with four helper plasmids (pHDM-VSV-G, pHDM-tat1b, pHDM-HgPM2, and pRC-CMVRaII), followed by viral supernatant collection after 72 h. To delete three *Tgfb* genes, WT or Lsd1 KO (clone g5-4) B16 cells were transduced with a mixture of lenti-CRISPR virus carrying respective gRNA with the addition of 8 μg/ml polybrene (Sigma-Aldrich, cat#H9268), and selected with 1 μg/ml puromycin for 2 days. Cells were then transferred into puromycin-free fresh medium and seeded at low density to allow colony formation from single cells. Colonies were then picked and expanded for knockout validation of all three *Tgfb* genes by sequencing of target genomic regions or ELISA.

Gene Ectopic Expression

For rescue assay, Lsd1 KO B16 cells were transduced with lentiviral pHAGE-CMV-Flag-HA-LSD1 and selected with puromycin for 2 weeks to obtain a stable cell line. To establish stable cell lines ectopically expressing dominant negative TGF-β receptor (TGFβRII-DN), cDNAs

were amplified from pCMV5-HA-TBRII (delta Cyt) (Addgene, cat#14051) and cloned into MSCV-PIG (Puro IRES GFP) retroviral vector (Addgene, cat#18751). Retrovirus carrying MSCV-PIG was used to transduce Lsd1 KO B16 cells, followed by puromycin selection for 2 weeks to obtain a stable cell line.

RNA Extraction and Real-Time qPCR

For total RNA extraction, supernatant was removed and cells were lysed by directly applying TRIzol (Life Technologies, cat#15596018) onto cells. RNA extraction was performed according to the manufacturer's instructions. The extracted RNA was reversely transcribed into cDNA using the PrimeScript™ RT Reagent Kit (TaKaRa, cat#RR037B). Briefly, RNA samples were first mixed with random 6-mers and oligo dT primers, denatured at 70 °C for 5 min and cooled down on ice, followed by the addition of buffer and reverse transcriptase. The reaction was then incubated at 37 °C for 30 min for reverse transcription and terminated at 85 °C for 15 sec. The obtained cDNA samples were diluted in H_2O and used for real-time quantitative PCR (qPCR). SYBR green (Life Technologies, cat#A25743) and gene specific primers (listed in **Supplementary Table S3**) were used for PCR amplification and detection on a QuantStudio 3 real-time PCR system (Applied Biosystems). The qPCR data were normalized to Gapdh and presented as fold changes of gene expression in the test sample compared to the control.

ELISA

The ELISA assay was performed with a Mouse TGF-beta 1 DuoSet ELISA kit (R&D Systems, cat#DY1679-05) according to the manufacturer's instructions. For measuring TGF-β1 secreted by cultured cells, cells were cultured for 24 h and changed to FBS-free medium for an additional 24 h, followed by supernatant collection and clearance by centrifugation. For measuring TGF-β1 protein level in implanted tumors, tumor masses were excised and snap-frozen in liquid nitrogen. Tumor samples were then homogenized in protein extraction buffer (100 mM Tris pH 7.4, 150 mM NaCl, 1 mM EGTA, 1 mM EDTA, 1% Triton X-100, 0.5% sodium deoxycholate and protease inhibitor cocktail) and incubated at 4 °C on a rotator for 30 min, followed by centrifugation to clear the lysate. Protein concentration in the lysate was quantified

by Bio-Rad protein assay (Bio-Rad, cat #5000006), to which TGF-β1 concentration was normalized.

Cell Colony Formation Assay

B16 cells in culture at 80% confluence were dissociated into single-cell suspension with trypsin, washed and re-suspended into fresh medium. The numbers of viable cells were counted and diluted appropriately for seeding on 12-well plates (200 cells per well). Cells were allowed to grow for 6 days, with an addition of fresh medium on day 3 without removing old medium. After that, the medium was removed and cells were stained with crystal violet solution (0.5% w/v crystal violet powder, 80% v/v H_2O and 20% v/v methanol).

Cell Cycle Analysis

B16 cells were harvested by trypsinization and fixed with 70% ethanol overnight. After fixation, cells were resuspended in 1X PBS, and permeabilized with 0.1% Triton X-100. Cells were then treated with RNase A (0.8 mg/ml, Thermo Fisher Scientific, cat#RN0531), stained with propidium iodide (Thermo Fisher Scientific, cat#P3566) and analyzed on a BD LSRII. The cell cycle profiles were analyzed to determine the fraction of cells in G1, S and G2/M phase using FlowJo.

Mouse Subcutaneous Tumor Models

Female wildtype C57BL/6 mice aged 6~10 weeks were purchased from The Jackson Laboratory and allowed to acclimate to housing conditions at the Boston Children's Hospital Animal Facility for one week. B6.129S2-Tcratm1Mom/J (TCRα KO) mice were originally purchased from The Jackson Laboratory (stock #002116) and bred at the Boston Children's Hospital Animal Facility. For experiments with B6.Cg-Tg(Cd4-TGFBR2)16Flv/J mice, those mice originally purchased from The Jackson Laboratory (stock #005551) were bred at the Boston Children's Hospital Animal Facility, and both female and male mice were used. Mice were anesthetized with isoflurane, shaved at right hind flank, and injected subcutaneously with

250,000 or 500,000 B16/F10 or D4m.3A tumor cells. Tumors were measured with a caliper every 2–3 days once palpable (long diameter and short diameter). Tumor volumes were calculated using the volume formula for an ellipsoid: $1/2 \times D \times d^2$ where D is the longer diameter and d is the shorter diameter. Mice were sacrificed when tumors reached 2000 mm^3 or upon ulceration/bleeding. All experimental mice were housed in specific pathogen–free conditions and all animal procedures were performed in accordance with animal care guidelines and with the prior approval by the Boston Children's Hospital Institutional Animal Care and Use Committee.

For antibody treatments, mice were administrated 100 μg antibody via intraperitoneal injection initiated based on a set day or set tumor volume and continued every 2~3 days as indicated. The following antibodies from BioXCell were used: anti-PD-1 (clone 29F.1A12), anti-TGF-β (clone 1D11) or rat IgG2a isotype control (clone 2A3). Prior to treatments mice were randomized such that treatment groups had similar average tumor volumes prior to treatment initiation.

For $CD4^+$ or $CD8^+$ T cell depletion, anti-CD4 depleting antibodies (clone GK1.5, BioXcell), anti-CD8α depleting antibodies (clone YTS169.4, BioXcell) or isotype control (clone LTF-2, BioXcell) were intraperitoneally injected into mice the day before tumor implantation at a dose of 200 μg, followed by injection of 100 μg every 3 days.

B16 Lung Metastasis Assay

200K B16/F10 cells with indicated genetic modifications were transferred intravenously into wildtype or TCRα KO female mice via tail vein injection. Lungs were removed 14 days post injection and fixed overnight in Fekete's solution. Visible metastases were counted in a blinded fashion.

Tumor Infiltrating Leukocyte Analysis by Flow Cytometry

Tumors were excised on day 14 post implantation and cut into 2 mm sized pieces in type I collagenase (Worthington Biochemical Corporation, cat# LS004194) and DNase I (Sigma-Aldrich, cat#10104159001). Samples were then incubated at 37°C for 30 minutes and passed through a 70 μm cell strainer. To enrich leukocytes, samples were spun through a Percoll (GE Healthcare Life Sciences, cat# 17-0891-01) gradient. Leukocytes were collected from the interface of the 40% and 70% Percoll gradient, stained, and analyzed for fluorescent markers. For cytokine staining, enriched leukocytes were stimulated in R10 medium with PMA (50 ng/ml, Sigma-Aldrich, cat#P1585) and ionomycin (500 ng/ml, Sigma-Aldrich, cat#I0634) in the presence of GolgiPlug (BD Biosciences, cat# 555029), followed by cellular surface staining and intracellular staining. The eBioscience Foxp3 Fixation/Permeabilization kit (cat# 00-5523-00) was used for intracellular staining. All antibodies were purchased from BioLegend, Thermo Fisher Scientific, R&D Systems or BD Biosciences: CD45.2 BV421 (clone 104), CD11b BV605 (clone M1/70), CD3e BV510 (clone 145-2C11), CD4 APC (clone RM4-5), CD8b APC-Cy7 (clone YTS156.7.7), CD8a BV605 (clone 53-6.7), Foxp3 PE (clone FJK-16s), Granzyme-B FITC (clone GB11), Ki-67 PerCP-Cy5.5 (clone B56), CD44 FITC (clone IM7), CD11c PE (clone N418), CD49b AF700 (clone DX5), Gr-1 APC-Cy7 (clone RB6-8C5), TNF-α FITC (clone MP6-XT22), IFN-γ PE (clone XMG1.2), PD-1 PE-Cy7 (clone 29F.1A12), CD86 AF700 (clone GL-1), CD103 FITC (clone 2E7), F4/80 PE-Cy7 (clone BM8), Arginase PE (clone A1exF5), CD64 FITC (clone X54-5/7.1), human TGFBRII PE (clone 25508).

Chromatin Immunoprecipitation (ChIP) Assay

B16 cells in culture was fixed in 1% formaldehyde (Thermo Fisher Scientific, cat#28908) for 10 min at room temperature on a shaker, followed by quenching in 125 mM glycine. Next, cells were washed twice with ice-cold 1X PBS and lysed in sonication buffer (50 mM HEPES pH7.9, 140 mM NaCl, 1 mM EDTA, 1% Triton X-100, 0.1% sodium deoxycholate, 0.2% SDS) supplemented with protease inhibitor, then subjected to sonication to obtain DNA fragments mostly between 300-800 bp. Subsequent procedures were conducted by following the Epigenesys protocol (https://www.epigenesys.eu/en/). The following antibodies were used for immunoprecipitation: anti-LSD1 (Abcam, cat#ab17721), anti-H3K4me1 (Abcam, cat#ab8895),

anti-H3K4me2 (EMD Millipore, cat#07-030), anti-H3K27ac (Active Motif, cat#39034) and rabbit normal IgG (Cell Signaling Technology, cat#2729).

RNA-seq Sample Processing

$CD8^+$ TILs were isolated from implanted B16 tumors on day 14 as described above. $CD8^+$ TILs from two individual tumors were combined as a biological replicate. $CD8^+$ TILs were stained with antibodies against CD45.2 (clone 104), TCRβ (clone H57-587), CD8 (clone YTS156.7.7) and 7-AAD Viability Staining Solution (BioLegend, cat# 420404) was used to exclude dead cells. The $CD45.2^+TCR\beta^+CD8^+$ cells were then sorted on a BD Aria. Approximately 30,000~70,000 sorted cells for each biological replicate were directly lysed in 1 ml TRIzol Reagent (Life Technologies, cat#15596018). After incubation for 5 mins, 0.2 ml chloroform was added and mixed by inverting the tubes several times. Samples were incubated for 2-3 mins and later centrifuged for 15 mins at 12,000g at 4 °C. The upper aqueous phase containing the RNA was collected and mixed with equal volume of 70% ethanol, which was then loaded into a spin column from a RNeasy Micro Kit (Qiagen, cat#74004) and subjected to RNA isolation according to the instruction manual. The on-column DNase digestion was conducted to eliminate DNA contamination.

Purified total RNA was quantified by Qubit (Invitrogen) and used for $polyA^+$ RNA isolation with a Nebnext® Poly(A) mRNA Magnetic Isolation Module (New England Biolabs, cat#E7490S) according to the manufacturer's instructions. The $polyA^+$ enriched RNA was then used to generate a directional RNA library with a NEBNext® Ultra™ II Directional RNA Library Prep Kit for Illumina® (New England Biolabs, cat#E7760L) and NEBNext® Multiplex Oligos for Illumina® (New England Biolabs, cat#E7335L) according to the manufacturer's instructions. Library concentrations and quality were assessed on a Bioanalyzer and by qPCR. The library was sequenced at Novaseq (Illumina) to generate reads from paired ends (2X150bp). The raw data are deposited at the Gene Expression Omnibus (GEO) under the subseries entry GSE161569.

RNA-seq Data Analyses and Functional Interpretations

The software hisat2 (version 2.1.0) was used to generate genome indices for mouse reference genome (GRCm38/mm10) and extract splice sites with gencode vM24 annotation. Next, the high quality paired-end RNA-seq reads were aligned to mouse reference genome, and the consequence of alignment served as the input for featureCounts to quantify raw read counts for protein-coding genes. We used R package DESeq2 (version 1.38.0) to identify differentially expressed genes (DEGs) between different groups. The raw read count per gene served as the input for DESeq2. Since three samples were collected in each condition, they were treated as biological replicates to improve the reliability of DEGs identification. Statistical tests for differential expression were based on a model using the negative binomial distribution. The reported statistical significances were corrected for multiple testing using the Benjamini-Hochberg procedure with a false discovery rate less than 0.05. In addition, to be called DEGs we required the fold change > 1.5. The up-regulated genes in QKO condition versus KO condition were queried to Gene Ontology Consortium for gene ontology enrichment assessment, with specification of biological process (BP).

Statistical Analyses

Statistical analyses were performed using GraphPad Prism 8 software and statistical significance was determined by $p < 0.05$. An unpaired Student's t test was used for comparisons between two groups and a two-way ANOVA was used for multiple comparisons of tumor growth. For comparing mouse survival curves, a Log-rank (Mantel-Cox) test was used.

REFERENCES

1. Ribas A, Wolchok JD. Cancer immunotherapy using checkpoint blockade. Science. 2018;359(6382):1350-5.
2. Sharma P, Hu-Lieskovan S, Wargo JA, Ribas A. Primary, Adaptive, and Acquired Resistance to Cancer Immunotherapy. Cell. 2017;168(4):707-23.
3. Ennishi D, Takata K, Beguelin W, Duns G, Mottok A, Farinha P, et al. Molecular and Genetic Characterization of MHC Deficiency Identifies EZH2 as Therapeutic Target for Enhancing Immune Recognition. Cancer Discov. 2019;9(4):546-63.
4. Burr ML, Sparbier CE, Chan KL, Chan YC, Kersbergen A, Lam EYN, et al. An Evolutionarily Conserved Function of Polycomb Silences the MHC Class I Antigen Presentation Pathway and Enables Immune Evasion in Cancer. Cancer Cell. 2019;36(4):385-401 e8.
5. Canadas I, Thummalapalli R, Kim JW, Kitajima S, Jenkins RW, Christensen CL, et al. Tumor innate immunity primed by specific interferon-stimulated endogenous retroviruses. Nat Med. 2018;24(8):1143-50.
6. Chiappinelli KB, Strissel PL, Desrichard A, Li H, Henke C, Akman B, et al. Inhibiting DNA Methylation Causes an Interferon Response in Cancer via dsRNA Including Endogenous Retroviruses. Cell. 2015;162(5):974-86.
7. Roulois D, Loo Yau H, Singhania R, Wang Y, Danesh A, Shen SY, et al. DNA-Demethylating Agents Target Colorectal Cancer Cells by Inducing Viral Mimicry by Endogenous Transcripts. Cell. 2015;162(5):961-73.
8. Sheng W, LaFleur MW, Nguyen TH, Chen S, Chakravarthy A, Conway JR, et al. LSD1 Ablation Stimulates Anti-tumor Immunity and Enables Checkpoint Blockade. Cell. 2018;174(3):549-63 e19.
9. Peng D, Kryczek I, Nagarsheth N, Zhao L, Wei S, Wang W, et al. Epigenetic silencing of TH1-type chemokines shapes tumour immunity and immunotherapy. Nature. 2015;527(7577):249-53.
10. Rabinovich GA, Gabrilovich D, Sotomayor EM. Immunosuppressive strategies that are mediated by tumor cells. Annu Rev Immunol. 2007;25:267-96.
11. Batlle E, Massague J. Transforming Growth Factor-beta Signaling in Immunity and Cancer. Immunity. 2019;50(4):924-40.
12. Thomas DA, Massague J. TGF-beta directly targets cytotoxic T cell functions during tumor evasion of immune surveillance. Cancer Cell. 2005;8(5):369-80.
13. Tauriello DVF, Palomo-Ponce S, Stork D, Berenguer-Llergo A, Badia-Ramentol J, Iglesias M, et al. TGFbeta drives immune evasion in genetically reconstituted colon cancer metastasis. Nature. 2018;554(7693):538-43.
14. Mariathasan S, Turley SJ, Nickles D, Castiglioni A, Yuen K, Wang Y, et al. TGFbeta attenuates tumour response to PD-L1 blockade by contributing to exclusion of T cells. Nature. 2018;554(7693):544-8.
15. Liu VC, Wong LY, Jang T, Shah AH, Park I, Yang X, et al. Tumor evasion of the immune system by converting CD4+CD25- T cells into CD4+CD25+ T regulatory cells: role of tumor-derived TGF-beta. J Immunol. 2007;178(5):2883-92.
16. Hinshelwood RA, Huschtscha LI, Melki J, Stirzaker C, Abdipranoto A, Vissel B, et al. Concordant epigenetic silencing of transforming growth factor-beta signaling pathway genes occurs early in breast carcinogenesis. Cancer Res. 2007;67(24):11517-27.

17. Matsumura N, Huang Z, Mori S, Baba T, Fujii S, Konishi I, et al. Epigenetic suppression of the TGF-beta pathway revealed by transcriptome profiling in ovarian cancer. Genome Res. 2011;21(1):74-82.
18. Shen J, Ju Z, Zhao W, Wang L, Peng Y, Ge Z, et al. ARID1A deficiency promotes mutability and potentiates therapeutic antitumor immunity unleashed by immune checkpoint blockade. Nat Med. 2018;24(5):556-62.
19. Pan D, Kobayashi A, Jiang P, Ferrari de Andrade L, Tay RE, Luoma AM, et al. A major chromatin regulator determines resistance of tumor cells to T cell-mediated killing. Science. 2018;359(6377):770-5.
20. Russo V, Protti MP. Tumor-derived factors affecting immune cells. Cytokine Growth Factor Rev. 2017;36:79-87.
21. Chen DS, Mellman I. Elements of cancer immunity and the cancer-immune set point. Nature. 2017;541(7637):321-30.
22. Sow HS, Ren J, Camps M, Ossendorp F, Ten Dijke P. Combined Inhibition of TGF-beta Signaling and the PD-L1 Immune Checkpoint Is Differentially Effective in Tumor Models. Cells. 2019;8(4):320.
23. Wang Y, Zhang H, Chen Y, Sun Y, Yang F, Yu W, et al. LSD1 is a subunit of the NuRD complex and targets the metastasis programs in breast cancer. Cell. 2009;138(4):660-72.
24. Ohkura N, Kitagawa Y, Sakaguchi S. Development and maintenance of regulatory T cells. Immunity. 2013;38(3):414-23.
25. Gorelik L, Flavell RA. Abrogation of TGFbeta signaling in T cells leads to spontaneous T cell differentiation and autoimmune disease. Immunity. 2000;12(2):171-81.
26. Jones PA, Ohtani H, Chakravarthy A, De Carvalho DD. Epigenetic therapy in immune-oncology. Nat Rev Cancer. 2019;19(3):151-61.
27. Ciardiello D, Elez E, Tabernero J, Seoane J. Clinical development of therapies targeting TGFbeta: current knowledge and future perspectives. Ann Oncol. 2020;31(10):1336-49.
28. Majello B, Gorini F, Sacca CD, Amente S. Expanding the Role of the Histone Lysine-Specific Demethylase LSD1 in Cancer. Cancers (Basel). 2019;11(3):324.
29. Pickup M, Novitskiy S, Moses HL. The roles of TGFbeta in the tumour microenvironment. Nat Rev Cancer. 2013;13(11):788-99.
30. Garber K. Companies waver in efforts to target transforming growth factor beta in cancer. J Natl Cancer Inst. 2009;101(24):1664-7.
31. Lan Y, Zhang D, Xu C, Hance KW, Marelli B, Qi J, et al. Enhanced preclinical antitumor activity of M7824, a bifunctional fusion protein simultaneously targeting PD-L1 and TGF-beta. Sci Transl Med. 2018;10(424):eaan5488.
32. Terabe M, Robertson FC, Clark K, De Ravin E, Bloom A, Venzon DJ, et al. Blockade of only TGF-beta 1 and 2 is sufficient to enhance the efficacy of vaccine and PD-1 checkpoint blockade immunotherapy. Oncoimmunology. 2017;6(5):e1308616.
33. Vanpouille-Box C, Diamond JM, Pilones KA, Zavadil J, Babb JS, Formenti SC, et al. TGFbeta Is a Master Regulator of Radiation Therapy-Induced Antitumor Immunity. Cancer Res. 2015;75(11):2232-42.

Figure Legends

Figure 1. LSD1 ablation-induced TGF-β production impedes anti-tumor T cell immunity. **A,** Real-time qPCR analysis of RNA expression of Tgfb subfamily genes in cultured scramble, Lsd1 KO and Lsd1 KO rescued with Flag-HA-LSD1 B16 cells (n=3). **B,** ELISA quantification of the total secreted TGF-β1 protein in the supernatant of cultured B16 cells with indicated genetic manipulations (n=3). **C,** Real-time qPCR analysis of Tgfb1 and Serpine1 expression in scramble and Rcor1 KO B16 cells (n=3). **D,** Real-time qPCR analysis of a panel of IFNs and ISGs in cultured scramble, Lsd1 KO and Lsd1/Tgfb QKO B16 cells (n=3). **E,** Immunoblot of RIG-I, a protein encoded by an ISG gene, *Ddx58*, in cultured B16 cells with indicated genetic manipulations. **F** and **G,** Tumor growth (**F**) and survival curves (**G**) of immunocompetent (wildtype) mice subcutaneously inoculated with scramble, Lsd1 KO, Lsd1/Tgfb QKO or Tgfb TKO B16 cells. **H,** ELISA quantification of total TGF-β1 protein in implanted B16 tumors of different genetic perturbations. **I** and **J,** Scramble and Lsd1/Tgfb QKO B16 tumor growth curves in TCRα knockout mice (**I**) or wildtype mice treated with CD4-depleting, CD8-depleting or isotype control antibodies (**J**). Data represent two to three independent experiments (**A-J**). Error bars represent standard deviation (SD) between sample triplicates in one experiment (**A-D**) or standard error of the mean (SEM) of individual mice per group in one experiment (**F, H-J**). *p<0.05, **p<0.01, ***p<0.001, ****p<0.0001, ns, not significant, as determined by unpaired t test (**A-D, H** and **I**), 2-way ANOVA (**F** and **J**) or log-rank test (**G**).

Figure 2. Abrogation of TGF-β induction unleashes T cell cytotoxicity in LSD1 null tumors. **A,** Numbers of tumor-infiltrating $CD8^+$ T cells in scramble, Lsd1 KO and Lsd1/Tgfb QKO B16 tumors analyzed by flow cytometry on day 14. **B-D,** Percentages of Ki-67^+ cells (**B**), PD-1^+

cells (**C**) and GzmB$^+$ cells (**D**) among CD8$^+$ TILs analyzed by flow cytometry. **E,** Mean fluorescence intensity (MFI) of GzmB in CD8$^+$GzmB$^+$ TILs. **F,** Volcano plots showing differential gene expression (fold change > 1.5 and adjusted $p < 0.05$ as the cutoff) in RNA-seq analysis of CD8$^+$ TILs isolated from scramble, Lsd1 KO, Lsd1/Tgfb QKO and Tgfb TKO B16 tumors (n=3 per group) on day 14. **G,** Heatmap of RNA-seq data depicting a list of differentially expressed genes (QKO versus KO) and their expression in CD8$^+$ TILs derived from four groups of tumors. **H,** Dot plot showing the enriched pathways of the upregulated genes in CD8$^+$ TILs isolated from QKO compared with KO B16 tumors. **I,** Bar plot of RNA-seq data depicting the relative expression of cytotoxic molecules in CD8$^+$ TILs isolated from KO, QKO and TKO compared with scramble B16 tumors. **J** and **K,** Expression of TNF-α (**J**) and IFN-γ (**K**) in CD8$^+$ TILs analyzed by intracellular staining and flow cytometry after re-stimulation with PMA/Ionomycin in the presence of GolgiPlug. Data represent two independent experiments (**A-E**, **J**, **K**) and error bars represent SEM of individual tumors per group in one experiment (**A-E**, **I-K**). *p<0.05, **p<0.01, $^{\#}$p.adj<0.05, $^{\#\#}$p.adj<0.01, $^{\#\#\#}$p.adj<0.001, ns, not significant, as determined by unpaired t test (**A-E, J, K**) or in DESeq2 (**I**).

Figure 3. TGF-β receptor signaling in $\alpha\beta$ T cells mediates the suppression of CD8$^+$ T cell cytotoxicity in LSD1 null tumors. **A,** Tumor growth curves of wildtype (WT) and CD4-dnTGFBRII (dnTβRII) transgenic mice subcutaneously inoculated with scramble, Lsd1 KO or Lsd1/Tgfb QKO B16 cells. **B** and **C,** Percentages of GzmB$^+$ cells among CD8$^+$ TILs in scramble (**B**), Lsd1 KO and Lsd1/Tgfb QKO B16 tumors (**C**) analyzed by intracellular staining and flow cytometry. **D** and **E,** Percentages of FOXP3$^+$ Treg cells among CD4$^+$ TILs in scramble (**D**), Lsd1 KO and Lsd1/Tgfb QKO B16 tumors (**E**) analyzed by intracellular staining and flow

cytometry. **F,** Flow cytometry analysis of ectopic TGFβRII-DN expression on the surface of Lsd1 KO B16 cells transduced with MSCV-PIG-TβRII-DN (DN) or empty vector (EV). **G,** Real-time qPCR analysis of Tgfb1 and Serpine1 expression in B16 cells with indicated genetic modifications (n=3). **H,** Tumor growth curves of immunocompetent mice subcutaneously inoculated with Lsd1 KO B16 cells stably expressing TGFβRII-DN (DN) or empty vector (EV). Data are pooled from two to three independent experiments (**A-E**) or represent two independent experiments (**F-H**). Error bars represent SEM of individual mice per group (**A-E, H**) or SD between sample triplicates (**G**). *p<0.05, **p<0.01, ***p<0.001, ****p<0.0001, ns, not significant, as determined by 2-way ANOVA (**A**) or unpaired t test (**B-E, G, H**).

Figure 4. Anti-PD-1 treatment eradicates LSD1 null tumors when TGF-βs are concurrently blocked. **A** and **B,** Tumor growth (**A**) and survival curves (**B**) of immunocompetent mice implanted with scramble or Lsd1/Tgfb QKO B16 tumor cells under different treatment. The anti-PD-1 or isotype control treatment was initiated based on a set tumor volume (~250 mm^3) and continued every other day for a total of four injections as indicated by black (scramble) and blue (QKO) arrows. **C,** Tumor growth curves of immunocompetent mice implanted with scramble or Lsd1 KO B16 tumor cells under different treatment. The anti-PD-1, anti-TGF-β, isotype control or combinatorial treatment was initiated based on a set tumor volume (~200 mm^3) and continued every three days for a total of two injections as indicated by black (scramble) and red (KO) arrows. **D** and **E,** Tumor growth (**D**) and survival curves (**E**) of immunocompetent mice implanted with scramble or Lsd1 KO D4m.3A tumor cells under different antibody treatment administered on day 12 and 15 for a total of two injections. **F,** Numbers of tumor-infiltrating $CD4^+$ T cells, $CD8^+$ T cells, $CD11b^+Gr\text{-}1^+$ MDSCs and $CD3e^-$

CD49b$^+$ NK cells in scramble and Lsd1 KO B16 tumors treated with indicated antibodies on day 13 and 15, and analyzed by flow cytometry on day 17. **G,** Percentages of GzmB$^+$ cells among CD8$^+$ TILs under different conditions analyzed by intracellular staining and flow cytometry. **H,** Relative MFI of GzmB in CD8$^+$GzmB$^+$ TILs under different conditions in comparison to control (scramble + isotype). **I** and **J,** Percentages of Ki-67$^+$ cells among CD8$^+$ TILs (**I**) and FOXP3$^+$ Treg cells among CD4$^+$ TILs (**J**) under different conditions analyzed by intracellular staining and flow cytometry. **K** and **L,** Percentages of GzmB$^+$ cells among CD8$^+$ TILs (**K**) and MFI of GzmB in CD8$^+$GzmB$^+$ TILs (**L**) isolated from scramble, Lsd1 KO, Tgfb TKO or Lsd1/Tgfb QKO B16 tumors with indicated antibody treatment on day 13 and 15, and analyzed by flow cytometry on day 17. Data represent two independent experiments (**A-E, I, K, L**) or are pooled from two independent experiments (**F-H, J**). Error bars represent SEM of individual mice per group (**A, C, D**, **F-L**). *p<0.05, **p<0.01, ***p<0.001, ****p<0.0001, ns, not significant, as determined by 2-way ANOVA (**A**, **C** and **D**), log-rank test (**B** and **E**) or unpaired t test (**F-L**).

Figure 1

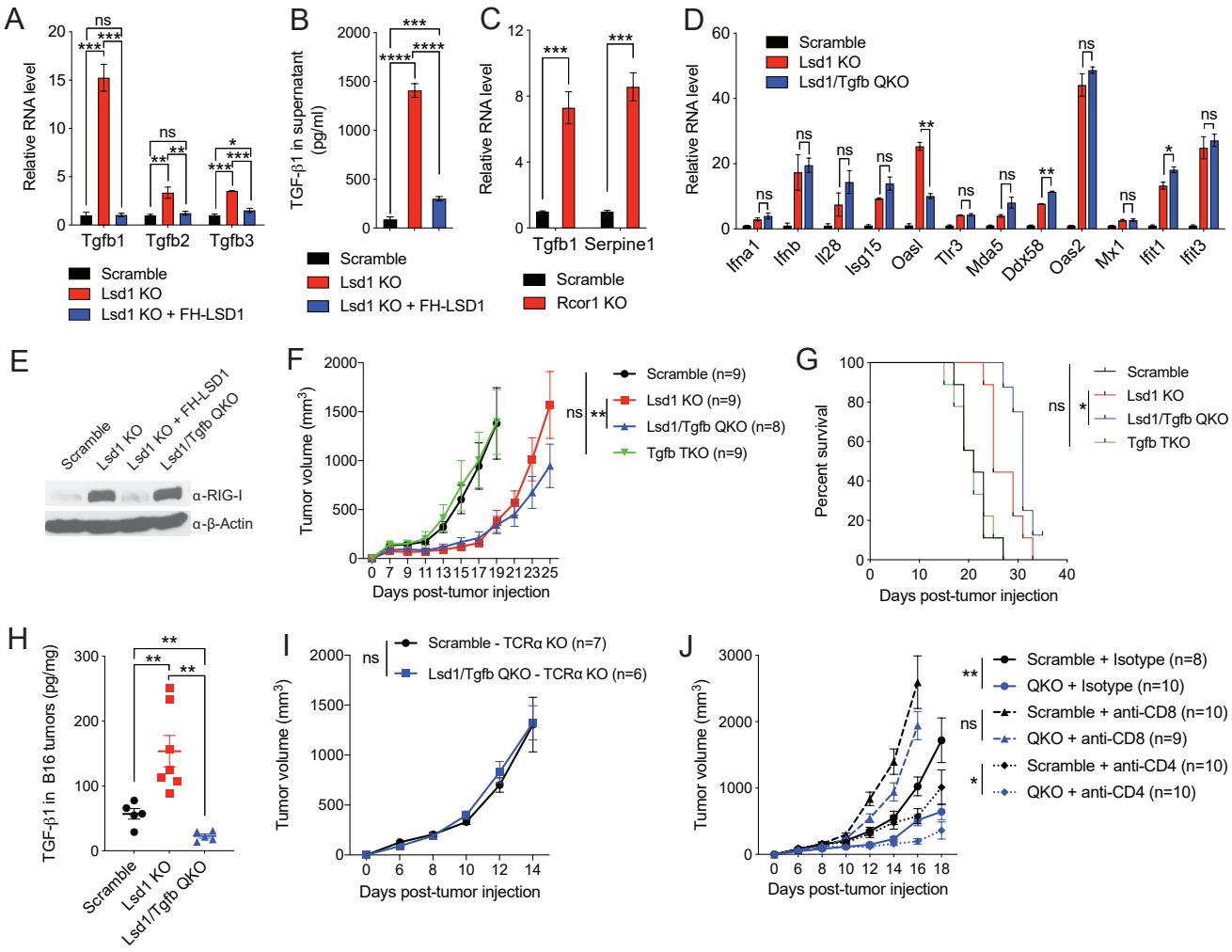
A
Relative RNA level
Tgfb1
Tgfb2
Tgfb3
Scramble
Lsd1 KO
Lsd1 KO + FH-LSD1
B
TGF-β1 in supernatant (pg/ml)
Scramble
Lsd1 KO
Lsd1 KO + FH-LSD1
C
Relative RNA level
Tgfb1
Serpine1
Scramble
Rcor1 KO
D
Relative RNA level
Scramble
Lsd1 KO
Lsd1/Tgfb QKO
Ifna1
Ifnb
Il28
Isg15
Oasl
Tlr3
Mda5
Ddx58
Oas2
Mx1
Ifit1
Ifit3
E
Scramble
Lsd1 KO
Lsd1 KO + FH-LSD1
Lsd1/Tgfb QKO
α-RIG-I
α-β-Actin
F
Tumor volume (mm3)
Days post-tumor injection
Scramble (n=9)
Lsd1 KO (n=9)
Lsd1/Tgfb QKO (n=8)
Tgfb TKO (n=9)
G
Percent survival
Days post-tumor injection
Scramble
Lsd1 KO
Lsd1/Tgfb QKO
Tgfb TKO
H
TGF-β1 in B16 tumors (pg/mg)
Scramble
Lsd1 KO
Lsd1/Tgfb QKO
I
Tumor volume (mm3)
Days post-tumor injection
Scramble - TCRα KO (n=7)
Lsd1/Tgfb QKO - TCRα KO (n=6)
J
Tumor volume (mm3)
Days post-tumor injection
Scramble + Isotype (n=8)
QKO + Isotype (n=10)
Scramble + anti-CD8 (n=10)
QKO + anti-CD8 (n=9)
Scramble + anti-CD4 (n=10)
QKO + anti-CD4 (n=10)

Figure 2

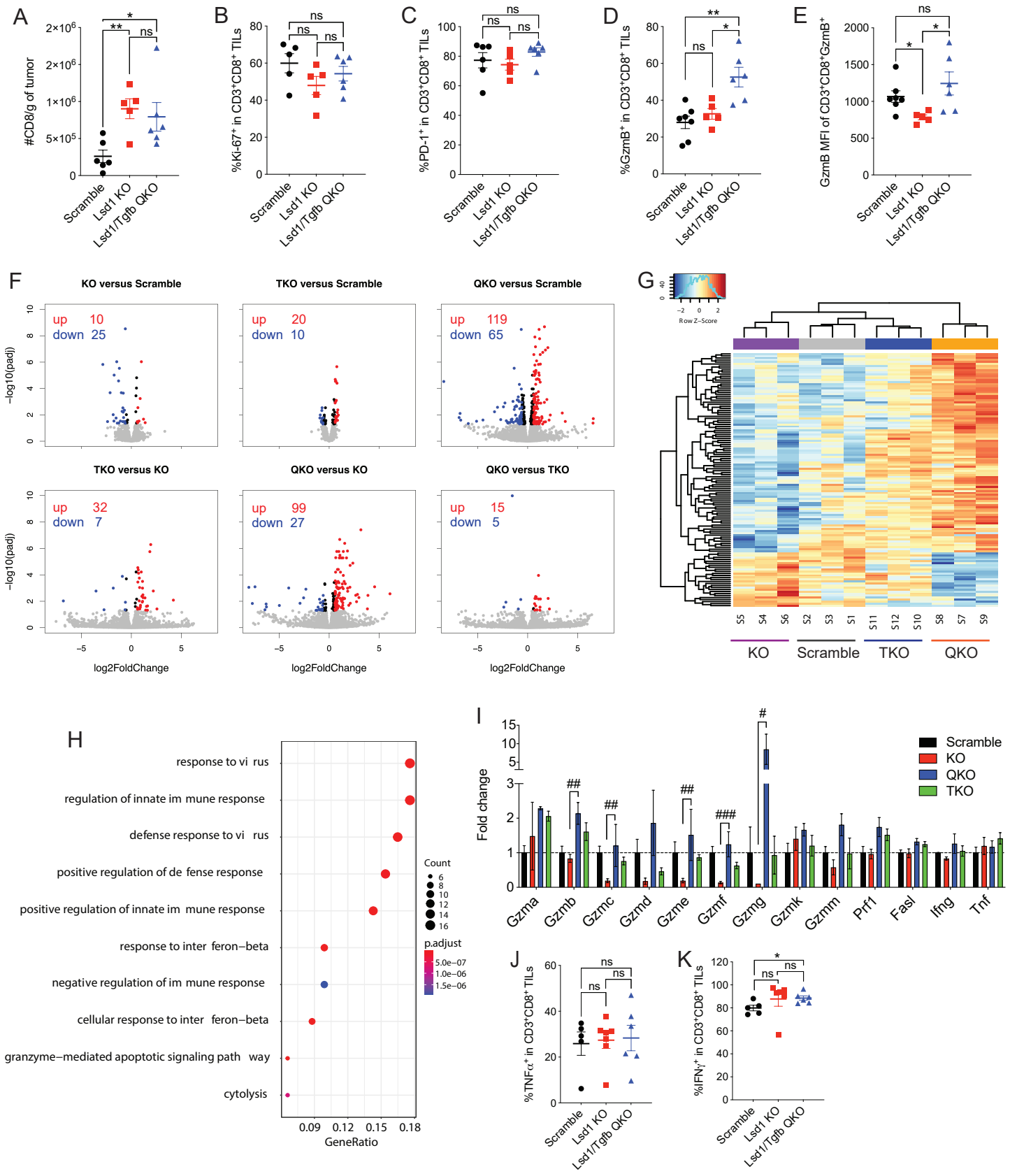
A
#CD8/g of tumor
Scramble
Lsd1 KO
Lsd1/Tgfb QKO
B
%Ki-67+ in CD3+CD8+ TILs
C
%PD-1+ in CD3+CD8+ TILs
D
%GzmB+ in CD3+CD8+ TILs
E
GzmB MFI of CD3+CD8+GzmB+
F
KO versus Scramble
up 10
down 25
TKO versus Scramble
up 20
down 10
QKO versus Scramble
up 119
down 65
TKO versus KO
up 32
down 7
QKO versus KO
up 99
down 27
QKO versus TKO
up 15
down 5
−log10(padj)
log2FoldChange
G
Row Z−Score
S5 S4 S6 S2 S3 S1 S11 S12 S10 S8 S7 S9
KO
Scramble
TKO
QKO
H
response to vi rus
regulation of innate im mune response
defense response to vi rus
positive regulation of de fense response
positive regulation of innate im mune response
response to inter feron−beta
negative regulation of im mune response
cellular response to inter feron−beta
granzyme−mediated apoptotic signaling path way
cytolysis
Count
p.adjust
GeneRatio
I
Fold change
Scramble
KO
QKO
TKO
Gzma
Gzmb
Gzmc
Gzmd
Gzme
Gzmf
Gzmg
Gzmk
Gzmm
Prf1
Fasl
Ifng
Tnf
J
%TNFα+ in CD3+CD8+ TILs
K
%IFNγ+ in CD3+CD8+ TILs

Figure 3

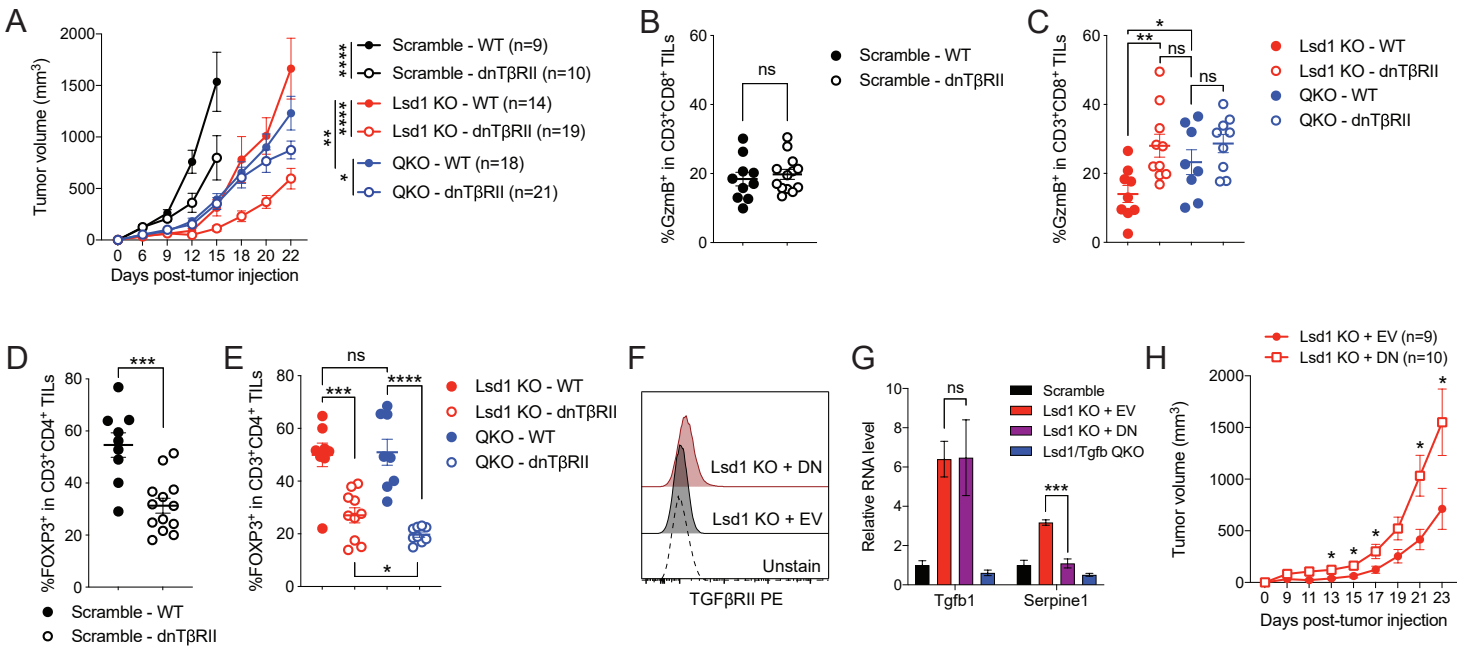
A
Tumor volume (mm3)
Days post-tumor injection
Scramble - WT (n=9)
Scramble - dnTβRII (n=10)
Lsd1 KO - WT (n=14)
Lsd1 KO - dnTβRII (n=19)
QKO - WT (n=18)
QKO - dnTβRII (n=21)
B
%GzmB+ in CD3+CD8+ TILs
ns
Scramble - WT
Scramble - dnTβRII
C
%GzmB+ in CD3+CD8+ TILs
Lsd1 KO - WT
Lsd1 KO - dnTβRII
QKO - WT
QKO - dnTβRII
D
%FOXP3+ in CD3+CD4+ TILs
Scramble - WT
Scramble - dnTβRII
E
%FOXP3+ in CD3+CD4+ TILs
Lsd1 KO - WT
Lsd1 KO - dnTβRII
QKO - WT
QKO - dnTβRII
F
Lsd1 KO + DN
Lsd1 KO + EV
Unstain
TGFβRII PE
G
Relative RNA level
Scramble
Lsd1 KO + EV
Lsd1 KO + DN
Lsd1/Tgfb QKO
Tgfb1
Serpine1
H
Lsd1 KO + EV (n=9)
Lsd1 KO + DN (n=10)
Tumor volume (mm3)
Days post-tumor injection

Figure 4

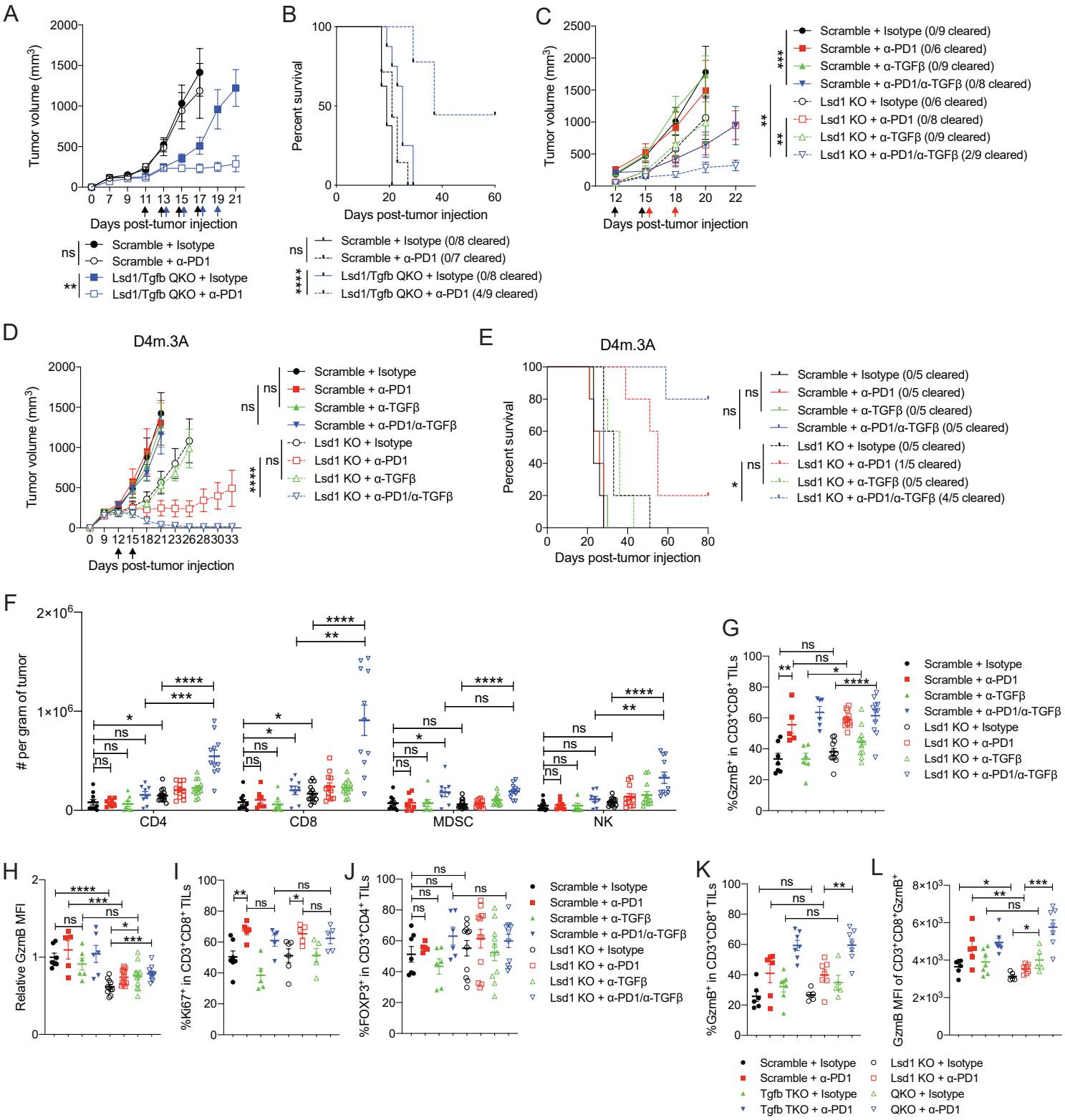
A
Tumor volume (mm3)
Days post-tumor injection
ns Scramble + Isotype
Scramble + α-PD1
** Lsd1/Tgfb QKO + Isotype
Lsd1/Tgfb QKO + α-PD1
B
Percent survival
Days post-tumor injection
ns Scramble + Isotype (0/8 cleared)
Scramble + α-PD1 (0/7 cleared)
**** Lsd1/Tgfb QKO + Isotype (0/8 cleared)
Lsd1/Tgfb QKO + α-PD1 (4/9 cleared)
C
Tumor volume (mm3)
Days post-tumor injection
*** Scramble + Isotype (0/9 cleared)
Scramble + α-PD1 (0/6 cleared)
Scramble + α-TGFβ (0/9 cleared)
Scramble + α-PD1/α-TGFβ (0/8 cleared)
** Lsd1 KO + Isotype (0/6 cleared)
Lsd1 KO + α-PD1 (0/8 cleared)
** Lsd1 KO + α-TGFβ (0/9 cleared)
Lsd1 KO + α-PD1/α-TGFβ (2/9 cleared)
D
D4m.3A
Tumor volume (mm3)
Days post-tumor injection
ns Scramble + Isotype
Scramble + α-PD1
Scramble + α-TGFβ
Scramble + α-PD1/α-TGFβ
**** Lsd1 KO + Isotype
Lsd1 KO + α-PD1
Lsd1 KO + α-TGFβ
Lsd1 KO + α-PD1/α-TGFβ
E
D4m.3A
Percent survival
Days post-tumor injection
ns Scramble + Isotype (0/5 cleared)
Scramble + α-PD1 (0/5 cleared)
Scramble + α-TGFβ (0/5 cleared)
Scramble + α-PD1/α-TGFβ (0/5 cleared)
* Lsd1 KO + Isotype (0/5 cleared)
Lsd1 KO + α-PD1 (1/5 cleared)
Lsd1 KO + α-TGFβ (0/5 cleared)
Lsd1 KO + α-PD1/α-TGFβ (4/5 cleared)
F
per gram of tumor
CD4
CD8
MDSC
NK
G
%GzmB+ in CD3+CD8+ TILs
Scramble + Isotype
Scramble + α-PD1
Scramble + α-TGFβ
Scramble + α-PD1/α-TGFβ
Lsd1 KO + Isotype
Lsd1 KO + α-PD1
Lsd1 KO + α-TGFβ
Lsd1 KO + α-PD1/α-TGFβ
H
Relative GzmB MFI
I
%Ki67+ in CD3+CD8+ TILs
J
%FOXP3+ in CD3+CD4+ TILs
K
%GzmB+ in CD3+CD8+ TILs
L
GzmB MFI of CD3+CD8+GzmB+
Scramble + Isotype
Scramble + α-PD1
Tgfb TKO + Isotype
Tgfb TKO + α-PD1
Lsd1 KO + Isotype
Lsd1 KO + α-PD1
QKO + Isotype
QKO + α-PD1